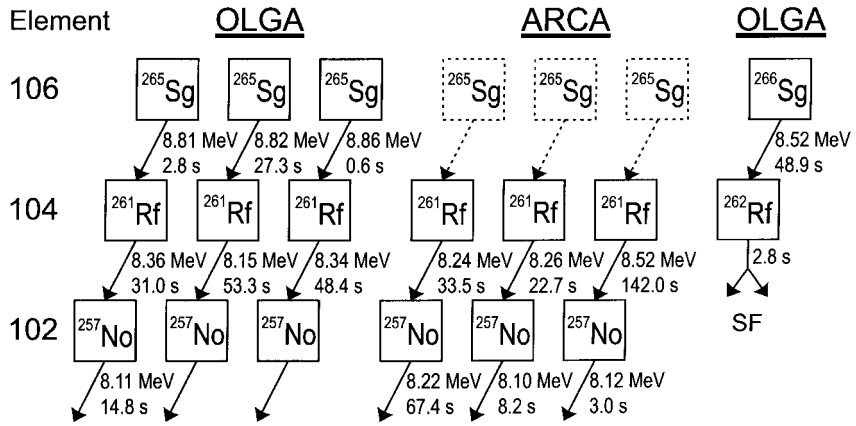


**Figure 3** The observed nuclear decay chains from the seaborgium isotopes $^{265}$Sg and $^{266}$Sg, which allowed an unambiguous identification of seaborgium after chemical separation with ARCA (automated rapid chemistry apparatus) and OLGA (on-line gas chemistry apparatus). The $\alpha$-decay energies are given in MeV, and the observed life-times in seconds.

through the column, given that both of these nuclides could only be present in the seaborgium fraction due to the α-decay of $^{265}$Sg. Isotopes of the elements 104 and 102 formed directly or from decay of seaborgium before chemical separation were chemically separated. With a 90% probability, the parent nuclei had already decayed into the daughter nucleus $^{261}$Rf in the time between the end of chemical separation and the commencement of measurement about 28 seconds later. This is very likely in view of the short life-times measured for the $^{265}$Sg decays with OLGA (Fig. 3).

The first liquid-chromatographic separation of element 106 shows that at least a substantial fraction of the formed seaborgium behaves similarly to its lighter homologues molybdenum and tungsten, that is, that its behaviour is typical of a hexavalent ion belonging to group 6 of the periodic table. Presumably, seaborgium forms $SgO_4^{2-}$ or a neutral complex.

Both our isothermal gas chromatographic and liquid chromatographic separations clearly indicate that seaborgium behaves similarly to its lighter homologues molybdenum and tungsten, and its behaviour is typical for a group 6 element of the period table. These results support the assumption that the chemistry of elements 107 to 112 will be homologous to that of the group 7 to 12 elements rhenium to mercury—if increasingly strong relativistic effects do not alter the chemical properties to such an extent that they are no longer predictable from such simple extrapolations, as seen for elements 104 and 105. □

Received 27 January; accepted 12 May 1997.


1. Fricke, B. & Greiner, W. On the chemistry of superheavy elements around Z = 164. *Phys. Lett. B* **30,** 317–319 (1969).
2. Desclaux, J.-P. & Fricke, B. Relativistic prediction of the ground state of atomic lawrencium. *J. Phys.* **41,** 943–946 (1980).
3. Glebov, V. A., Kasztura, L., Nefedov, V. S. & Zhuikov, B. L. Is element 104 (kurchatovium) a p-element? II. Relativistic calculations of the electronic atomic structure. *Radiochim. Acta* **46,** 117–121 (1989).
4. Johnson, E., Fricke, B., Keller, O. L., Nestor, C. W. & Tucker, T. C. Ionization potentials and radii of atoms and ions of element 104 (unnilquadium) and of hafnium (2+) derived from multiconfiguration Dirac-Fock calculations. *J. Chem. Phys.* **93,** 8041–8050 (1990).
5. Eliav, E., Kaldor, U. & Ishikawa, Y. Ground state electron configuration of rutherfordium: role of dynamic correlation. *Phys. Rev. Lett.* **74,** 1079–1082 (1995).
6. Pyykkö, P. Relativistic effects in structural chemistry. *Chem. Rev.* **88,** 563–594 (1988).
7. Pershina, V. G. Electronic structure and properties of the transactinides and their compounds. *Chem. Rev.* **96,** 1977–2101 (1996).
8. Hofmann, S. *et al*. The new element 112. *Z. Phys. A* **354,** 229–230 (1996).
9. Zvara, I., Belov, V. Z., Domanov, V. P. & Shalaevskii, M. R. Chemical isolation of nilsbohrium as ekatantalum in the form of the anhydrous bromide. II. Experiments with a spontaneously fissioning isotope of nilsbohrium. *Sov. Radiochem.* **18,** 328–334 (1976).
10. Gregorich, K. E. *et al*. Aqueous chemistry of element 105. *Radiochim. Acta* **43,** 223–231 (1988).
11. Kratz, J. V. *et al*. Chemical properties of element 105 in aqueous solution: halide complex formation and anion exchange into triisooctyl amine. *Radiochim. Acta* **48,** 121–133 (1989).
12. Gäggeler, H. W. *et al*. Gas phase chromatography experiments with bromides of tantalum and element 105. *Radiochim. Acta* **57,** 93–100 (1992).
13. Gäggeler, H. W. On-line gas chemistry experiments with transactinide elements. *J. Radioanal. Nucl. Chem.* **183,** 261–271 (1994).
14. Czerwinski, K. R. *et al*. Solution chemistry of element 104: Part I. Liquid–liquid extractions with triisoctylamine. *Radiochim. Acta* **64,** 23–28 (1994); Solution chemistry of element 104: Part II. Liquid–liquid extractions with tributylphosphate. *Radiochim. Acta* **64,** 29–35 (1994).
15. Türler, A. *et al*. On-line gas phase chromatography with chlorides of niobium and hahnium (element 105). *Radiochim. Acta* **73,** 55–66 (1996).
16. Kadkhodayan, B. *et al*. On-line gas chromatographic studies of chlorides of rutherfordium and homologs Zr and Hf. *Radiochim. Acta* **72,** 169–178 (1996).
17. Türler, A. Gas phase chemistry experiments with transactinide elements. *Radiochim. Acta* **72,** 7–17 (1996).
18. Schädel, M. Chemistry of the transactinide elements. *Radiochim. Acta* **70/71,** 207–223 (1996).
19. Hoffman, D. C. Chemistry of the heaviest elements. *Radiochim. Acta* **72,** 1–6 (1996).
20. Zimmermann, H. P. *et al*. Chemical properties of element 105 in aqueous solution: back extraction from triisooctyl amide into 0.5 M HCl. *Radiochim. Acta* **60,** 11–16 (1993).
21. Zvara, I. *et al*. Gas chromatography and thermochromatography in the study of transuranium elements. *Sov. Radiochem.* **16,** 709–715 (1974).
22. Lougheed, R. W. *et al*. in *Proc. Int. Conf. Actinides-93* (eds Clark, D. L., Hobart, D. E. & Fuger, F.) 161 (Elsevier, Amsterdam, 1994); *J. Alloy Compounds* **213/214,** 61–66 (1994).
23. Lazarev, Yu. A. *et al*. Discovery of enhanced nuclear stability near the deformed shells N = 162 and Z = 108. *Phys. Rev. Lett.* **73,** 624–627 (1994).
24. Schädel, M. *et al*. First aqueous chemistry with seaborgium (element 106). *Radiochim. Acta* (in the press).
25. Timokhin, S. N., Yakushev, A. B., Honggui Xu, Perelygin, V. P. & Zvara, I. Chemical identification of element 106 by thermochromatography. *J. Radioanal. Nucl. Chem. Lett.* **212,** 31–34 (1996).
26. Schädel, M. *et al*. ARCA II—a new apparatus for fast, repetitive HPLC separations. *Radiochim. Acta* **48,** 171–176 (1989).
27. Tytko, K.-H. & Gras, D. in *Gmelin, Handbook of Inorganic Chemistry, Molybdenum* Suppl. Vol. B 3b (Springer, Heidelberg, 1989).
28. Pershina, V. & Fricke, B. The electronic structure of the group 6 oxyanions $[MO_4]^{2-}$, where M = Cr, Mo, W, and element 106. *Radiochim. Acta* **65,** 13–17 (1994).


**Acknowledgements.** We are indebted to the Division of Chemical Sciences, Office of Basic Energy Research, US Department of Energy, for making the $^{248}$Cm target material through the transplutonium element production program at the Oak Ridge National Laboratory. We also thank the staff and crew of the GSI UNILAC, the TRIGA Mainz reactor, the Philips-cyclotron at PSI, and the MPI Heidelberg tandem accelerator for their help. This work was supported in part by the Bundesministerium für Bildung, Wissenschaft, Forschung und Technologie (BMBF), the Swiss National Science Foundation, and the Chemical Sciences Division of the Office of Basic Energy Sciences, US Department of Energy.

Correspondence should be addressed to M.S. (e-mail: m.schaedel@gsi.de).

# Vegetation and climate change in northwest America during the past 125 kyr

**Cathy Whitlock & Patrick J. Bartlein**

*Department of Geography, University of Oregon, Eugene, Oregon 97403, USA*

**Vegetation records spanning the past 21 kyr in western North America display spatial patterns of change that reflect the influence of variations in the large-scale controls of climate[1]. Among these controls are millennial-scale variations in the seasonal cycle of insolation and the size of the ice sheet, which affect regional climates directly through changes in temperature and net radiation, and indirectly by shifting atmospheric circulation. Longer vegetation records provide an opportunity to examine the regional response to different combinations of these large-scale controls, and whether non-climatic controls are important. But most of the longer North American records[2,3] are of insufficient quality to allow a robust test, and the long European records[4–9] are in regions where the vegetation response to climate is often**

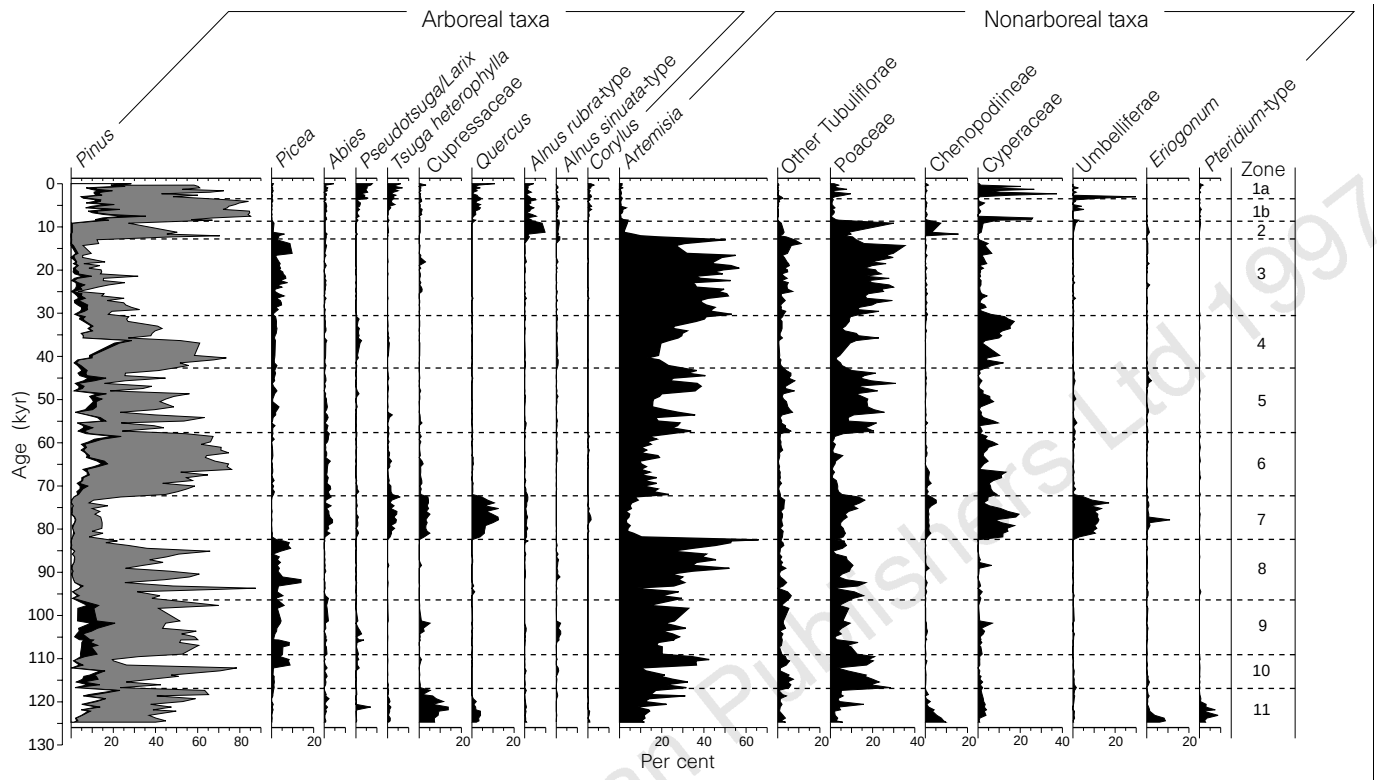


**Figure 1** Pollen percentage diagram of selected taxa from Carp Lake cores 90 and 93. *Pinus* includes diploxylon-type pollen (open curve) from *P. contorta* or *P. ponderosa*, haploxylon-type pollen (black curve) from *P. monticola* or *P. albicaulis*, and indeterminate *Pinus* pollen (shaded curve). A minimum of 350 terrestrial pollen grains was counted for each level and used as the pollen sum in calculating percentages.

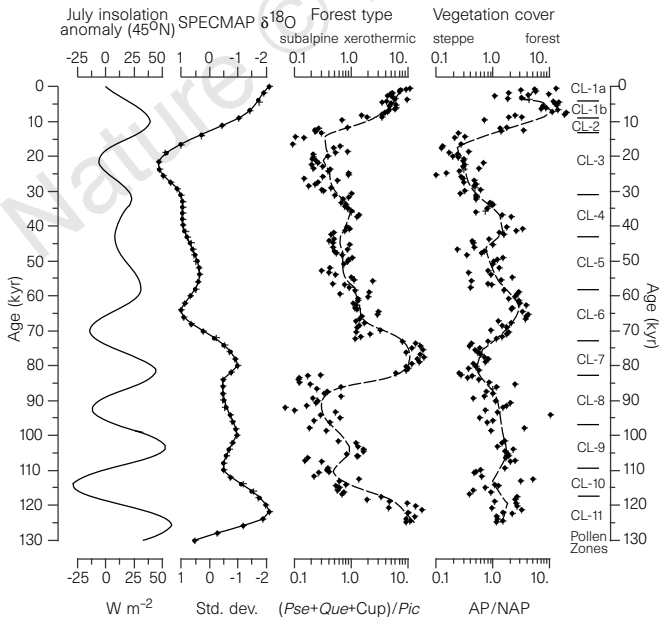


**Figure 2** Large-scale controls (July insolation anomalies at latitude 45° N and global ice volume) and Carp Lake vegetation indices. The ratios of the sum of *Pseudotsuga/Larix*, *Quercus* and Cupressaceae pollen percentages to *Picea* pollen percentages (*Pse* + *Que* + Cup/*Pic*) and of total arboreal to total non-arboreal pollen (AP/NAP) provide an indication of vegetation type and openness. The smoothed curves were drawn using a 'lowess' procedure[30].

**difficult to separate from the response to ecological and anthropogenic controls. Here we present a 125-kyr record of vegetation and climate change for the forest/steppe border of the eastern Cascade Range, northwest America. Pollen data disclose alternations of forest and steppe that are consistent with variations in summer insolation and global ice-volume, and vegetational transitions correlate well with the marine isotope-stage boundaries. The close relationship between vegetation and climate beyond the Last Glacial Maximum provides evidence that climate variations are the primary cause of regional vegetation change on millennial timescales, and that non-climatic controls are secondary.**

Regional vegetation history is generally regarded as a response to climate variations operating on different spatial and temporal scales[10]. One approach to understanding this hierarchy is the comparison of model simulations and data syntheses (for example, palaeoclimate model simulations of the past 21 kyr, produced by general circulation models, are compared with palaeoenvironmental maps constructed from palaeoecological data[11]). In northwest America, such comparisons reveal the influence of the Laurentide ice sheet and the seasonal cycle of insolation on regional climate[1]. Model simulations of full-glacial conditions[12,13] suggest that the ice sheet caused cooling of the northern mid-latitudes, steepened the latitudinal temperature gradient, and shifted the jet stream south of its present position. In addition, glacial anticyclonic circulation led to weakened westerlies, prevailing easterlies, and enhanced cold dry conditions along the southern ice margin. Simulations of the late-glacial period (16–10 kyr ago) suggest that a smaller ice sheet caused cool humid conditions as a result of a latitudinal temperature depression and a northwards shift of the jet. In the early Holocene

**Table 1 Ages and tephra information used to establish age–depth relations at Carp Lake**

| Depth* (m) | Uncalibrated $^{14}$C age (yr BP) | Calibrated $^{14}$C age (kyr)† | Lab no., tephra identification‡, or $\delta^{18}$O age equivalent | Core |
|---|---|---|---|---|
| 1.3 | 0 | 0 | Sediment surface | 90 |
| 2.15–2.16 | 3,450 ± 450 | 3.691 | Mt St Helens, Ye | 85 |
| 3.10–3.20 | 5,820 ± 50 | 6.667 | QL-1640 | 85 |
| 3.64–3.68 | 6,800 ± 200 | 7.581 | Mazama ash | 85 |
| 3.70–3.77 | 8,760 ± 40 | 9.754 | WIS-1460 | 85 |
| 3.82–3.92 | 9,470 ± 100 | 10.472 | WIS-1468 | 85 |
| 4.46–4.56 | 9,730 ± 400 | 10.961 | QL-1641 | 85 |
| 5.61–5.71 | 16,050 ± 400 | 18.925 | QL-1642 | 85 |
| 6.15–6.25 | 19,790 ± 190 | 23.45 | Beta-57036 | 90 |
| 6.76–6.86 | 21,100 ± 400 | 24.706 | QL-1643 | 85 |
| 8.30–8.40 | 26,200 ± 200 | 29.59 | QL-1646 | 85 |
| 9.10–9.20 | 32, 700 ± 450 | 35 | QL-1603 | 85 |
| 9.25–9.35 | 32, 760 ± 420 | 35 | Beta-57037 | 90 |
| 19.11–19.50 | ~100,000 | 100§ | Mt St Helens, WA-5C | 90 |
| 15.15 | | 73.9 | Stage 4/5a | 93 |
| 23.15 | | 125 | Stage 5e | 93 |

The following are regression equations:

$$\text{Age (kyr)} = -5.9284 + 4.1052\text{depth} + 0.0095\text{depth}^2 + 0.0032\text{depth}^3 \quad (1)$$

$$\text{Age (kyr)} = -3.3742 + 2.6245\text{depth} + 0.2186\text{depth}^2 - 0.0040\text{depth}^3 \quad (2)$$

Equation (2) incorporates $\delta^{18}$O ages for the pollen equivalents of stage 4/5a boundary and stage 5e (see ref. 18).
* Radiocarbon dates and tephra dates were used from core 85 (ref. 14) to a core depth of 9.8 m (below water surface), core 90 to a depth of 20.19 m, and core 93 from 20.19 to 23.15 m. Correlation among cores was based on lithology.
† Radiocarbon yr were converted to calendar yr (kyr) by use of the CALIB3 program for the past 20,000 $^{14}$C-yr BP (ref. 27), the U-Th calibration for ages between 20,000 and 30,000 $^{14}$C-yr BP (ref. 28), and the geomagnetic record for the period from 30,000 to 50,000 $^{14}$C-yr BP (ref. 29). Tephra ages are reported in refs 15, 16.
‡ Tephra identifications provided by A. Sarna-Wojcicki, US Geol. Survey.
§ Based on unpublished data (A. Sarna-Wojcicki) and extrapolation from a series of thermoluminescence (TL) dates in a nearby loess section (ref. 16). The age assignment is preliminary until further dating is conducted.

epoch, greater-than-present summer insolation increased summer temperatures, decreased effective precipitation, and indirectly strengthened the eastern Pacific subtropical high-pressure system, which intensified drought.

Comparisons between model results and data for the past 21 kyr encompass only a small subset of the large-scale variations that have occurred in the Quaternary period. Records that preserve evidence of the consequences of combinations of large-scale controls before the Last Glacial Maximum offer an alternative way to examine the hierarchy of controls of past climate variations. In such an approach, the past 21 kyr offer hypotheses about the relative influence of ice-sheet size and insolation variations that can be tested with the record from earlier periods.

A pollen record from Carp Lake (latitude 45° 55′ N, longitude 120° 53′ W, altitude 714 m above sea level), a crater lake in the eastern Cascade Range, provides a vegetation history of the past 125 kyr. The site lies at the lower altitudinal limit of *Pinus ponderosa* forest near *Artemisia* steppe, which is a sensitive ecotone for recording past variations in temperature and effective precipitation. Cores were collected in 1985[14], 1990 and 1993 to yield a 23.15-m-long record, and pollen was analysed from 196 samples taken at regular intervals. A preliminary age versus depth relationship was established based on radiocarbon dates and the ages of tephra layers[15,16] in the cores (Table 1, equation (1)). The pollen percentage record was divided into assemblage zones based on a constrained cluster analysis[17] (Fig. 1). Pollen zone boundaries were assigned independently of the marine $\delta^{18}$O stratigraphy[18], yet their ages matched the isotopic stage boundaries surprisingly well. The original chronology was revised by incorporating in the regression analysis the ages of marine isotope stage boundary 4/5a and the height of stage 5e (Table 1, equation (2)).

Interpretations of past vegetation and climate rested on a comparison of the pollen stratigraphy with modern pollen spectra[19], vegetation[20], and climate[20] (Table 2). Ratios of *Pseudotsuga* + *Quercus* + Cupressaceae/Picea provided information on forest type, with high values indicating low-elevation forest and warm, effectively dry conditions. These taxa were chosen because their pollen distribution today is sharply delimited by elevation, unlike *Pinus*, *Artemisia*, *Alnus* and *Tsuga*, which have widely dispersed pollen. Arboreal/non-arboreal pollen ratios were an index of vegetation cover and were used to separate periods of forest from steppe or tundra.

The pollen record is composed of taxa that grow today in the Cascade Range and Columbia basin. The previous interglaciation (CL-11) was characterized by open forests of *Pinus*, *Quercus* and *Juniperus* and by steppe; climate during this time was warmer and drier than most of the Holocene. Alternations of open *Pinus* and *Pinus-Picea* forest and closed mixed-conifer forest occurred from 83 to 117 kyr ago (CL-8 to CL-10) during cooler-than-present conditions. An open forest of *Pseudotsuga* or *Larix*, *Tsuga*, *Abies* (probably *A. grandis*), *Quercus* and Cupressaceae was present between 73 and 83 kyr ago (CL-7). The presence of *Quercus*, Chenopodiineae, and steppe herbs suggests that summers were warm, and the expansion of *Tsuga*, *Abies* and Poaceae indicates increased summer moisture. Cool conditions during the early and middle Wisconsin interval (CL-6 to CL-4) supported mixed conifer forests of *Pinus*, *Picea* and sometimes *Pseudotsuga* or *Larix*. The last glaciation (CL-3) featured cold dry steppe, and an expansion of *Picea* in the late-glacial. Temperate steppe was present in the early Holocene (CL-2), and Carp Lake dried intermittently[14]. The middle Holocene (CL-1b) was characterized by *Pinus* forest, and modern vegetation was established in the past 3,900 yr (CL-1a).

The close agreement between the pollen zonation and the marine $\delta^{18}$O stratigraphy, which is a proxy for global ice volume, suggests that vegetation changes were controlled by global variations in the climate system. Most of the variability at Carp Lake relates to the slowly changing insolation and ice-volume record, leaving little to be accounted for by higher-frequency variations, such as Heinrich events[21]. The synchroneity of the changes also suggests negligible lags between large-scale climatic forcing and local vegetational response. Apparently, species kept pace with millennial-scale climate changes by expanding their ranges short distances from discontinuous refugia.

Shifts in forest types parallel variations in both the marine $\delta^{18}$O record[22] and anomalies in July insolation[23] for the past 125 kyr (Fig. 2). Periods of low ice volume and summer insolation maxima featured xerothermic taxa. Periods of moderate ice volume and summer insolation minima supported subalpine conifers. When the combination of large-scale controls was unique, so too was the vegetation. For example, anomalous conditions during the full-glacial

**Table 2 Carp Lake vegetation and climate history**

| Pollen zone age and depth | Oxygen isotope stage and age (ref. 18) | Vegetation | Inferred climate |
|---|---|---|---|
| CL-1a 0–3.9 kyr (1.30–2.35 m) | 1 0–14.1 kyr | Development of the modern forest in the Late Holocene. *Pinus ponderosa* and *Pseudotsuga menziesii* became the dominant trees, with *Alnus*, *Corylus* and other shrubs. Mesic locations supported *Abies grandis*, *Pinus monticola* and *Tsuga heterophylla*. *Quercus* woodland was established at lower treeline. Poaceae pollen indicates the establishment of grassland at lower elevations and in forest openings. | Modern |
| CL-1b 3.9–9.1 kyr (2.35–3.70 m) | | Middle Holocene forest of *Pinus ponderosa* and *Quercus* woodland. | Warmer drier than present |
| CL-2 9.1–13.2 kyr (3.70–4.65 m) | | Early Holocene steppe vegetation with Poaceae and Chenopodiineae. *Alnus* was present in riparian settings. | Warmer drier than present |
| CL-3 13.2–30.9 kyr (4.65–8.25 m) | 2 14.1–27.6 kyr | Cold steppe with *Artemisia*, Poaceae and herbs during the full-glacial period. Temperate aquatic taxa (for example, *Nuphar*, *Sparganium*-type, *Myriophyllum*, *Polygonum amphibium*-type and *Typha*) are absent. *Polygonum bistortoides*-type pollen (not shown) indicates subalpine or alpine conditions. Populations of *Picea engelmannii* near the site, especially in late-glacial period. | Coldest driest period |
| CL-4 30.9–43.1 kyr (8.25–10.4 m) | 3 27.6–58.9 kyr | Open forest with mixture of low- and high-elevation species. *Picea* and *Abies* present in mesic settings, and lower or drier forests supported *Pinus contorta* or *P. ponderosa*, *Pseudotsuga* or *Larix occidentalis*, and *Abies grandis*. *Picea* and *Artemisia* pollen are more abundant at the bottom of the zone. | Cooler drier than present |
| CL-5 43.1–58.0 kyr (10.4–12.85 m) | | Open forest or forest-steppe vegetation, dominated by *Pinus ponderosa* and/or *P. contorta* with lesser amounts of *Picea* and *Abies*. Pollen of Poaceae, *Artemisia* and other herbs suggests forest openings or nearby steppe. | Cooler than present, relatively humid |
| CL-6 58.0–72.7 kyr (12.85–15.15 m) | 4 58.9–73.9 kyr | Closed *Pinus* forest with some *Picea* and *Abies*. *Artemisia* percentages indicate dry forest openings. | Cooler drier than present |
| CL-7 72.7–82.8 kyr (15.15–16.70 m) | 5a 73.9–85.1 kyr | Open forest of *Pseudotsuga/Larix*, *Tsuga heterophylla*, *Abies*, *Quercus* and Cupressaceae; the first four taxa are typical of low elevations in the western Cascade Range. Cupressaceae pollen may have come from *Thuja plicata* or *Chamaecyparis nootkatensis*, both mesophytes, or *Juniperus occidentalis*, a xerophyte. Chenopodiineae, Poaceae, *Pteridium*, Umbelliferae and *Eriogonum* were present. | Warmer wetter summers than present |
| CL-8 82.8–96.8 kyr (16.70–18.83 m) | 5b 85.1–93.6 kyr | Open forest of *Picea engelmannii*, *Pinus contorta* and possibly *P. ponderosa*. *Alnus sinuata* grew in areas of seepage. *Artemisia* percentages imply nearby steppe or forest openings. | Cooler than present, dry |
| CL-9 96.8–109.5 kyr (18.83–20.75 m) | 5c 93.6–107 kyr | Closed forest with *Pinus*, *Pseudotsuga/Larix*, *Abies* and *Picea*, similar to montane forests in the Cascades and northeastern Oregon. *Pinus* pollen was probably from *P. contorta*, *P. ponderosa*, and *P. monticola* or *P. albicaulis*. | Warmer summers than present, cool humid winters |
| CL-10 109.5–117.3 kyr (20.75–21.95 m) | 5d 107–116.7 kyr | Open *Pinus* forest with *Picea*, *Abies*, *Artemisia* and Poaceae. | Cooler than present, humid |
| CL-11 117.3–124.9 kyr (21.95–23.15 m) | 5e 116.7–133 kyr | Open forest during previous interglaciation. *Pinus* is from *P. ponderosa* or *P. contorta*. *Quercus* suggests dry woodland at lower elevations. Cupressaceae is ascribed to *Juniperus*. Chenopodiineae, *Eriogonum*, *Artemisia* and Poaceae values imply steppe element. *Brasenia schreberi* (not shown) occurs in this zone and the Holocene only. | Warmer drier than Holocene |

led to no-analogue steppe (CL-3). During the last half of the previous interglaciation, summer insolation exceeded that of the early Holocene and global ice volume was at its lowest; these conditions fostered a warm, dry climate and an expansion of xerophytic forest (CL-11). The interglacial period had greater forest cover than the early Holocene, and the record does not show the strong climate variability during stage 5e noted in the Greenland ice-core record[24] and some European pollen records[25]. Stage 5a featured an unusual combination of high summer insolation, modest global ice volumes, and cooler-than-present sea surface temperatures in the north Pacific Ocean[26]. High summer insolation probably increased growing-season temperature, but a cool ocean and a steepened temperature gradient may have lessened drought and allowed the eastward shift of mesophytic taxa at the expense of *Pinus* and *Artemisia* (CL-7).

Differences in vegetational succession among interglacial and interstadial periods have received considerable attention, particularly in Europe where several long pollen sequences have been described[4–9]. The differences are often attributed to singular circumstances during particular periods, including non-climatic factors such as refugial location, dispersal-rate differences among taxa, and biotic interactions. Like European records, Carp Lake shows the individualistic response of vegetation during the Late Quaternary, but the close correspondence of the vegetational variations and the large-scale controls of climate indicates that non-climatic variables were of little or no importance on millennial timescales. Carp Lake offers compelling evidence that interglacial and interstadial vegetation assemblages owe their distinctiveness primarily to the effects of global variations in climate. □

Received 23 December 1996; accepted 13 May 1997.


1. Thompson, R. E., Whitlock, C., Bartlein, P. J., Harrison, S. & Spaulding, W. G. in *Global Climates since the Last Glacial Maximum* (eds Wright, H. E. Jr *et al.*) 468–513 (Univ. Minnesota, Minneapolis, 1993).
2. Heusser, L. E. & King, J. E. in *Vegetation History* (eds Huntley, B. & Webb, T.) 193–236 (Kluwer, Dordrecht, 1988).
3. Adam, D. P. Correlations of the Clear Lake, California, core CL-73-7 pollen sequence with other climate records. *Geol. Soc. Am. Spec. Pap.* **214,** 81–96 (1988).
4. Watts, W. A. in *Vegetation History* (eds Huntley, B. & Webb, T.) 155–192 (Kluwer, Dordrecht, 1988).
5. Watts, W. A., Allen, J. R. M. & Huntley, B. Vegetation history and paleoclimate of the last glacial-interglacial period at Lago Grande di Monticchio, southern Italy. *Quat. Sci. Rev.* **15,** 113–154 (1996).
6. Pons, A., Guiot, J., de Beaulieu, J. L. & Reille, M. Recent contributions to the climatology of the last glacial interglacial cycle based on French pollen sequences. *Quat. Sci. Rev.* **11,** 439–448 (1992).
7. Guiot, J., Pons, A., de Beaulieu, J. L. & Reille, M. A 140,000-year continental climate reconstruction from two European pollen records. *Nature* **338,** 309–313 (1989).
8. Tzekadis, P. C., Bennett, K. D. & Magri, D. Climate and the pollen record. *Nature* **370,** 513 (1994).
9. Tzekadis, P. C. & Bennett, K. D. Interglacial vegetation succession: a view from southern Europe. *Quat. Sci. Rev.* **14,** 967–982 (1995).
10. Huntley, B. & Webb, T. *Vegetation History* (Kluwer, Dordrecht, 1988).
11. Wright, H. E. Jr *et al. Global Climates since the Last Glacial Maximum* (Univ. Minnesota, Minneapolis, 1993).

12. Kutzbach, J. E. & Guetter, P. J. The influence of changing orbital patterns and surface boundary conditions on climate simulations for the past 18,000 years. *J. Atmos. Sci.* **43,** 1726–1759 (1986).
13. Hall, N. M. J., Valdes, P. J. & Dong, B. The maintenance of the last great ice sheets: a UGAMP GCM study. *J. Clim.* **9,** 1004–1009 (1996).
14. Barnosky, C. W. A record of late-Quaternary vegetation from the southwestern Columbia Basin, Washington. *Quat. Res.* **23,** 109–122 (1985).
15. Sarna-Wojcicki, A. J. in *Late Quaternary Environments of the United States* Vol. 2 (ed. Wright, H. E. Jr) 52–77 (Univ. Minnesota, Minneapolis, 1983).
16. Berger, G. W. & Busacca, A. J. Thermoluminescence dating of Late Pleistocene loess and tephra from eastern Washington and southern Oregon and implications for the eruptive history of Mount St. Helens. *J. Geophys. Res.* **100,** 22361–22374 (1995).
17. Grimm, E. C. in *Vegetation History* (eds Huntley, B. & Webb, T.) 53–76 (Kluwer, Dordrecht, 1988).
18. Martinson, D. G. *et al.* Age dating and the orbital theory of the ice ages: development of a high resolution 0 to 300,000-year chronostratigraphy. *Quat. Res.* **27,** 1–29 (1987).
19. Mack, R. N. & Bryant, V. M. Jr Modern pollen spectra from the Columbia Basin, Washington. *Northwest Sci.* **48,** 183–194 (1974).
20. Franklin, J. F. & Dyrness, C. T. *Natural Vegetation of Oregon and Washington* (Oregon State Univ., Corvallis, 1988).
21. Bond, G. *et al.* Correlations between climate records from North Atlantic sediments and Greenland ice. *Nature* **365,** 143–147 (1993).
22. Imbrie, J. *et al.* in *Milankovitch and Climate* (eds Berger, A., Imbrie, J., Hays, J., Kukla, G. & Saltzman, B.) 269–305 (Reidel, Dordrecht, 1984).
23. Berger, A. & Loutre, M. F. Insolation values for the last 10 million years. *Quat. Sci. Rev.* **10,** 297–317 (1991).
24. Greenland Ice-core Project (GRIP) Members. Climate instability during the last interglacial period recorded in the GRIP ice core. *Nature* **364,** 203–207 (1993).
25. Thouveny, N. *et al.* Climate variations in Europe over the past 140 kyr deduced from rock magnetism. *Nature* **371,** 503–506 (1994).
26. Morley, J. J., Pisias, N. G. & Leinen, M. Late Pleistocene time series of atmospheric and oceanic variables recorded in sediments from the subarctic Pacific. *Paleoceanography* **2,** 49–62 (1987).
27. Stuiver, M. & Reimer, P. J. Extended $^{14}C$ data base and revised CALIB 3.0 $^{14}C$ age calibration program. *Radiocarbon* **35,** 215–230 (1993).
28. Bard, E., Hamelin, B., Fairbanks, R. G. & Zindler, A. Calibration of the $^{14}C$ timescale over the past 30,000 years using mass spectrometric U-Th ages from Barbados corals. *Nature* **345,** 405–410 (1990).
29. Mazaud, A., Laj, C., Bard, E., Arnold, M. & Tric, A. E. Geomagnetic field control of $^{14}C$ production over the last 80 kyr: implications for the radiocarbon time-scale. *Geophys. Res. Lett.* **18,** 1885–1888 (1991).
30. Cleveland, W. S. *Visualizing Data* (Hobard, Summit, 1993).

**Acknowledgements.** We thank A. Sarna-Wojcicki for tephra identifications, R. J. Nickmann for help with the pollen analysis, and J. Guiot and R. E. Gresswell for reviews. The work was supported by the NSF and the Westinghouse-Hanford Paleoclimate Program.

Correspondence and requests for materials should be addressed to C.W. (e-mail: whitlock@oregon.uoregon.edu).

# Endemic African mammals shake the phylogenetic tree

**Mark S. Springer*, Gregory C. Cleven*, Ole Madsen†, Wilfried W. de Jong†‡, Victor G. Waddell§, Heather M. Amrine* & Michael J. Stanhope§**

* *Department of Biology, University of California, Riverside, California 92521, USA*
† *Department of Biochemistry, University of Nijmegen, PO Box 9101, 6500 HB Nijmegen, The Netherlands*
‡ *Institute for Systematics and Population Biology, University of Amsterdam, PO Box 94766, 1090GT Amsterdam, The Netherlands*
§ *Biology and Biochemistry, Queen's University, 97 Lisburn Road, Belfast BT9 07BL, UK*

**The order Insectivora, including living taxa (lipotyphlans) and archaic fossil forms, is central to the question of higher-level relationships among placental mammals[1]. Beginning with Huxley[2], it has been argued that insectivores retain many primitive features and are closer to the ancestral stock of mammals than are other living groups[3]. Nevertheless, cladistic analysis suggests that living insectivores, at least, are united by derived anatomical features[4]. Here we analyse DNA sequences from three mitochondrial genes and two nuclear genes to examine relationships of insectivores to other mammals. The representative insectivores are not monophyletic in any of our analyses. Rather, golden moles are included in a clade that contains hyraxes, manatees, elephants, elephant shrews and aardvarks. Members of this group are of presumed African origin[5,6]. This implies that there was an extensive African radiation from a single common ancestor that gave rise to ecologically divergent adaptive types. 12S ribosomal RNA transversions suggest that the base of this radiation occurred during Africa's window of isolation in the Cretaceous period before land connections were developed with Europe in the early Cenozoic era.**

Relationships among orders of placental mammals have proved difficult to resolve[1]. To extend the available mitochondrial (mt) sequences, a 2.6-kilobase (kb) segment containing the 12S rRNA, valine transfer RNA, and 16S rRNA genes was sequenced for nine taxa to generate a data set that is representative of 12 of the 18 placental orders and all three insectivore suborders[4]. Phylogenetic analyses provide strong support for well-established mammalian clades such as carnivores, hominoids, and Cetacea plus Artiodactyla (Fig. 1a). In agreement with other molecular studies[7–10] that included an assortment of taxa, most interordinal associations are not resolved at bootstrap values >75%. However, the mtDNA data do provide strong support for the association of the two paenungulates (hyrax, manatee) together, and of these with elephant shrews, aardvarks and golden moles (Fig. 1a and Table 1). The association of hyraxes with proboscideans and sirenians was suggested by Cope[11]. A competing hypothesis is an association of hyraxes with perissodactyls[12]. Our results agree with earlier protein[13,14] and DNA studies[7–10] supporting Cope's paenungulate hypothesis. In addition to bootstrap support, T-PTP[15] and Kishino–Hasegawa[16] tests also support paenungulate monophyly (Table 2). Anatomical data provide some evidence that aardvarks and/or elephant shrews may be related to paenungulates[17,18] but suggest other hypotheses as well: for example, six osteological features are putative synapomorphies uniting elephant shrews with lagomorphs and rodents[19]. All the available sequence data, including amino-acid sequences[13,14], DNA sequences for three nuclear genes[8–10], and the present mitochondrial genes, support an association of aardvarks and elephant shrews with paenungulates. What is most unexpected is that golden moles, a family of insectivores, are also part of this clade. 12S rRNA sequences earlier suggested an association of golden moles with paenungulates, but did not provide convincing bootstrap support for this hypothesis[7]. Our expanded data set demonstrates that insectivores are not monophyletic (Table 2)

**Table 1 Bootstrap support for select clades based on different methods**

| | Clade | |
|---|---|---|
| | Paenungulata | Paenungulata + aardvark + elephant shrew +golden mole |
| Mitochondrial DNA | | |
| Parsimony | 99 | 95 |
| Transversion parsimony | 64 | 90 |
| Minimum evolution | | |
| Tamura–Nei I | 100 | 92 |
| Tamura–Nei II | 100 | 78 |
| Logdet | 99 | 90 |
| Maximum likelihood | 100 | 100 |
| vWF | | |
| Parsimony | | |
| All positions | 49 | 99 |
| 1st and 2nd positions | 24 | 65 |
| 3rd positions | 51 | 93 |
| Transversion parsimony | 30 | 95 |
| Minimum evolution | | |
| Tamura–Nei I | 37 | 99 |
| Tamura–Nei II | 30 | 99 |
| Logdet | 43 | 97 |
| Maximum likelihood | 78 | 100 |
| A2AB | | |
| Parsimony | | |
| All sites | 71 | 88 |
| 1st and 2nd positions | 49 | 81 |
| 3rd positions | 31 | 67 |
| Transversion parsimony | 71 | 54 |
| Minimum evolution | | |
| Tamura–Nei I | 83 | 84 |
| Tamura–Nei II | 28 | 25 |
| Logdet | 79 | 78 |
| Maximum likelihood | 81 | 89 |

Only two of the three paenungulate orders were represented among the mitochondrial and A2AB sequences. Tamura–Nei[27] I and II distances were calculated by using an equal-rates assumption and a gamma-distribution of rates, respectively.